JACS
JOURNAL OF THE AMERICAN CHEMICAL SOCIETY
Article
pubs.acs.org/JACS

Optically Triggered Stepwise Double-Proton Transfer in an Intramolecular Proton Relay: A Case Study of 1,8-Dihydroxy-2-naphthaldehyde

Chia-Yu Peng,[†] Jiun-Yi Shen,[‡] Yi-Ting Chen,[‡] Pei-Jhen Wu,[‡] Wen-Yi Hung,[§] Wei-Ping Hu,*[,†] and Pi-Tai Chou*[,‡]

[†]Department of Chemistry and Biochemistry, National Chung Cheng University, Chia-Yi 62102, Taiwan R.O.C.

[‡]Department of Chemistry and Center for Emerging Material and Advanced Devices, National Taiwan University, Taipei 10617, Taiwan R.O.C.

[§]Institute of Optoelectronic Sciences, National Taiwan Ocean University, Keelung 20224, Taiwan R.O.C.

Supporting Information

ABSTRACT: 1,8-Dihydroxy-2-naphthaldehyde (**DHNA**), having doubly intramolecular hydrogen bonds, was strategically designed and synthesized in an aim to probe a long-standing fundamental issue regarding synchronous versus asynchronous double-proton transfer in the excited state. In cyclohexane, **DHNA** shows the lowest lying $S_0 \rightarrow S_1$ ($\pi-\pi^*$) absorption at ~400 nm. Upon excitation, two large Stokes shifted emission bands maximized at 520 and 650 nm are resolved, which are ascribed to the tautomer emission resulting from the first and second proton-transfer products, denoted by TA* and TB*, respectively. The first proton transfer (**DHNA*** → TA*) is ultrafast (< system response of 150 fs), whereas the second proton transfer is reversible, for which the rates of forward (TA* → TB*) and backward (TA* ← TB*) proton transfer were determined to be $(1.7\ \text{ps})^{-1}$ and $(3.6\ \text{ps})^{-1}$, respectively. The fast equilibrium leads to identical population lifetimes of ~54 ps for both TA* and TB* tautomers. Similar excited-state double-proton transfer takes place for **DHNA** in a single crystal, resulting in TA* (560 nm) and TB* (650 nm) dual-tautomer emission. A comprehensive 2D plot of reaction potential energy surface further proves that the sequential two-step proton motion is along the minimum energetic pathway firmly supporting the experimental results. Using **DHNA** as a paradigm, we thus demonstrate unambiguously a stepwise, proton-relay type of intramolecular double-proton transfer reaction in the excited state, which should gain fundamental understanding of the multiple proton transfer reactions.

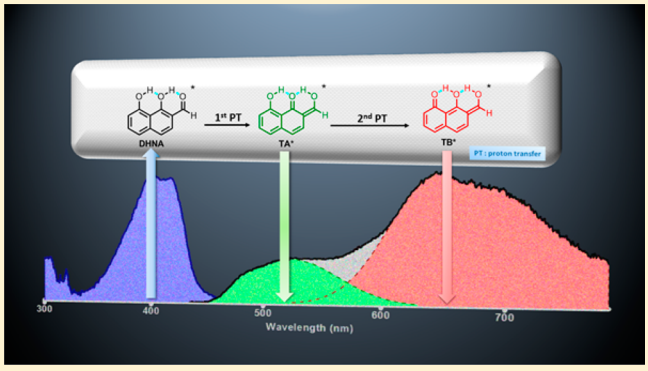

INTRODUCTION

Most excited-state intramolecular proton transfer (ESIPT) reactions refer to the single-proton transfer event. Upon electronic excitation, the transfer of a proton (or hydrogen atom) takes place via the existence of an intramolecular hydrogen bond between proton donor (O−H or N−H) and acceptor (carbonyl oxygen or nitrogen). In most cases,[1] this process results in a tautomer species possessing a drastically different electron density distribution (compared to the normal form). The tautomer thus exhibits large Stokes shifted emission, which has received intensive attention in both fundamental exploration[2−10] and potential applications.[10−18]

However, such a single-proton transfer event may not be sufficient to mimic the proton transfer reaction in biological systems, which may frequently be associated with multiple-proton transfer reactions, incorporating the migration of protons via a series of proton relays bridged by the hydrogen bonds, among which the proton transfer in hydroxylic solvents, the so-called Grotthuss mechanism,[19] is a prototype. Unfortunately, up to this stage, ESIPT systems capable of incorporating more than a single-proton transfer are very rare. Here we exclude those systems for which the proton transfer in the excited state is catalyzed by the protic solvent molecules.[6,20−28] Accordingly, one famous example may be ascribed to the hydrogen-bonded (H-bonded) dimer of 7-azaindole (Scheme 1). 7-Azaindole H-bonded dimer undergoes a switch of two symmetric protons in the excited state, denoted as excited-state double-proton transfer (ESDPT), the associated double-proton transfer reaction dynamics of which has been a core subject during the past several decades.[29−32] Unfortunately, such an externally H-bonded dimer has an ill-defined structure. This, together with the structure perturbation by solvent molecules, made the associated mechanism unclear, and it has been the

Received: August 13, 2015
Published: October 23, 2015

DOI: 10.1021/jacs.5b08562
J. Am. Chem. Soc. 2015, 137, 14349−14357

Scheme 1. Excited-State Double-Proton Transfer[a]

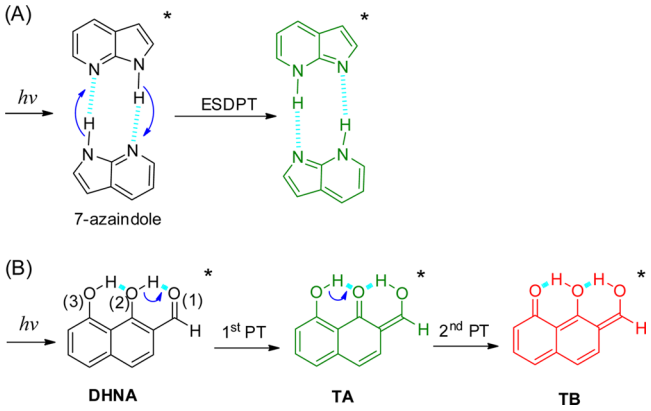

[a]Excited-state double-proton transfer (ESDPT) in (A) 7-azaindole dimer and (B) **DHNA** presented in this study. Note that the arrow in blue denotes the migration of proton. PT, proton transfer.

subject of a long-standing debate regarding synchronous (concerted) versus asynchronous (nonconcerted and/or stepwise) types of double proton-transfer. The other representative case is [2,2′-bipyridyl]-3,3′-diol (BP-(OH)$_2$),[33−36] which contains two channels of ESDPT with concerted (one-step) and/or sequential (two-step) proton transfer. The latter has been concluded to be a more favorable pathway according to the computational approach.[36] A very recent example is credited to 7-hydroxyquinoline-8-carboxylic acid, in which intramolecular double-proton transfer takes place via the assistance of the built-in carboxylic acid group.[37] Unfortunately, because all these cases did not show distinct emission associated with first and second proton transfers, experimentally whether it is one-step or stepwise process for the transfer of two protons remains unclear.

Experimentally, to the best of our knowledge, none of the systems so far have provided definitive reaction pathways regarding the double- or multiple-proton transfer in the excited state. In an aim to probe this crucial fundamental issue regarding the possible stepwise double-proton transfer in the excited state, 1,8-dihydroxy-2-naphthaldehyde[38,39] (**DHNA**, Scheme 1), possessing double intramolecular hydrogen bonds, and its derivatives were strategically designed and synthesized. The Results and Discussion section clearly demonstrate for the first time a case of stepwise, relay-type intramolecular double-proton transfer in the excited state.

RESULTS AND DISCUSSION

Syntheses and Structural Characterization. In this work, **DHNA** was prepared from commercially available starting material naphthalene-1,8-diol (**1**) following the literature[38,39] (Scheme 2). **1** was reacted with NaH and chloromethyl methyl ether by protecting the hydroxyl protons to form 1,8-bis(methylmethoxy)naphthalene (**2**). The addition of the aldehyde group on **2**, forming 1,8-bis(methoxymethoxy)-2-naphthaldehyde (**3**), was accomplished using *n*-BuLi and TMEDA, followed by DMF with good yield. Deprotection of **3** under an acid condition gave the designated compound **DHNA**. Definitive proof of **DHNA** is given by the X-ray structure analysis. Chart 1 depicts the single-crystal structure and the packing of **DHNA** in the unit cell. Monoclinic **DHNA** single crystals (Tables S1−S3 and Figure S1) belong to the space group of $P2(1)/c$, with cell parameters of a = 8.4818(10)

Scheme 2. (A) Synthesis of DHNA and (B) Structure of HN12

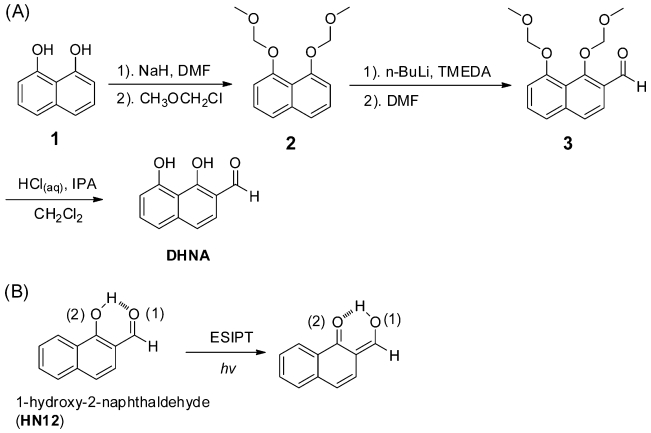

Chart 1. X-ray Structure and Packing of DHNA[a]

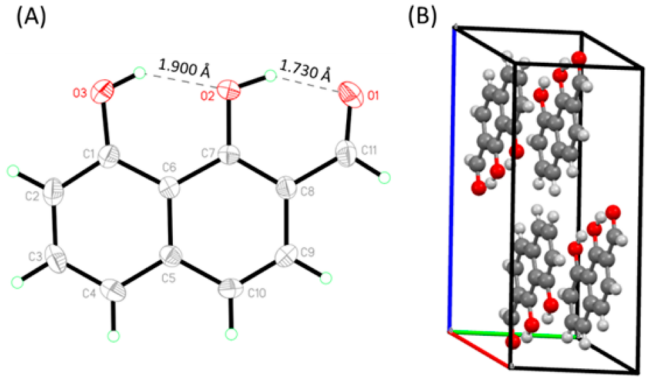

[a](A) X-ray structure of **DHNA**, with thermal ellipsoids drawn at 50% probability level. (B) View of the packing of **DHNA** in the unit cell.

Å, b = 6.7611(8) Å, c = 14.9995(17) Å, $\alpha = \gamma = 90°$, and β = 105.17°. According to Chart 1, the distances between the two hydrogen bonds of O(2)H···O(1) and O(3)H···O(2) are estimated to be 1.73 and 1.90 Å, respectively, strongly supporting the existence of dual intramolecular hydrogen bonds under a double six-membered-ring configuration. In good agreement with this observation, the ^{1}H NMR spectrum of **DHNA** in $CDCl_3$ (Figure S2) showed two sharp proton peaks at 14.2 and 9.4 ppm, assigned to the two −OH protons, manifesting the dual intramolecular H-bonding formation for **DHNA**. Chemically, the stronger H-bond leads to more downfield ^{1}H NMR shift. In accord with the H-bonding distance revealed in X-ray structure analysis, the 14.2 and 9.4 ppm proton peaks are assigned to the −O(2)H and −O(3)H protons H-bonded to carbonyl O(1) and hydroxyl O(2), respectively (Chart 1 and Scheme 1). This assignment is further supported by the comparison with the control compound, 1-hydroxy-2-naphthaldehyde (**HN12**, Scheme 2B), which shows a sharp proton peak at 12.6 ppm (Figure S2), pointing to a stronger intramolecular H-bond formation. Details of the synthesis and characterization are elaborated upon in the Experimental Section.

Steady-State and Dynamics Studies in Solution. **DHNA** exhibits the lowest lying absorption band maximized at 400 nm ($\varepsilon \approx 1.1 \times 10^4$ M^{-1}cm^{-1}), which is reasonably attributed to a $\pi-\pi^*$ transition. Upon electronic excitation, **DHNA** clearly exhibits dual-emission bands maximized at 520

DOI: 10.1021/jacs.5b08562
J. Am. Chem. Soc. 2015, 137, 14349−14357

and 650 nm in cyclohexane (Figure 1). Monitoring the 520 and 650 nm emission regions showed the corresponding excitation

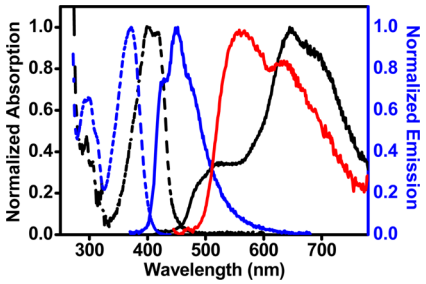

Figure 1. Absorption (dashed lines) and emission (solid lines) spectra of **DHNA** (black) and **3** (blue) in cyclohexane and the emission spectrum of single crystal **DHNA** at room temperature (red solid line).

spectra to be identical (Figure S3) and also the same as the absorption spectrum, indicating that the two emission bands share the same ground-state origin. The differences in peak frequency between absorption and emission, defined as the Stokes shift, are as large as 5800 and 9615 cm^{-1} for 520 and 650 nm bands, respectively. For comparison, proton transfer is prohibited in **3** (Scheme 2) because of the lack of a proton donor. Accordingly, **3** exhibits solely one emission band ($\lambda_{max} \approx$ 450 nm, Figure 1), showing a normal Stokes shift and mirror image with respect to the lowest-lying absorption band (λ_{max} = 365 nm). Note that this 450 nm emission band is apparently missing in the case of **DHNA**.

The above steady-state spectroscopic results led to the proposal that excited-state intramolecular proton transfer takes place in **DHNA**, resulting in two types of proton transfer tautomers (isomers); hence, dual emission is maximized at 520 and 650 nm. The molecular structure of each isomer can be inferred from the control compound, **HN12**, which has been reported to undergo ESIPT from −O(2)H to the carbonyl oxygen (O(1)),[40,41] yielding a distinct O(2)-keto tautomer emission at ∼480 nm. The spectral similarity makes it reasonable to ascribe the 520 nm emission in **DHNA** to an O(2)-keto-like tautomer (TA*; * denotes the electronically excited state). Accordingly, the 650 nm emission most plausibly originates from the O(3)-keto tautomer (TB*) possessing extensive elongation of the π conjugation (Schemes 1 and 3). Because the excitation of **DHNA** is mainly from an aldehyde form configured with a relay of O(2)−H and O(3)−H in H-bonds (denoted by N in Scheme 3), double-proton transfer must take place in the excited state to rationalize the TB* generation. The interplay between one-proton and two-proton transfer in the excited state, resulting in TA* and TB*, is then of prime fundamental interest. Single (TA*) and double (TB*) proton transfer may proceed via two separated pathways with a distinct branching ratio, a stepwise two-proton transfer may take place, sequentially yielding TA* and TB*, or even more complicated multiple pathways. Insight into this important fundamental is gained from the time-resolved emission kinetics and theoretical approach elaborated upon below.

We made attempts to further resolve the dynamics of ESDPT for **DHNA** by using the femtosecond fluorescence upconversion technique. The results shown in Figure 2 and Table S4 reveal that the TA* emission monitored at 520 nm (λ_{ex} = 400 nm, 120 fs) consists of a fast relaxation decay (1.1 ± 0.2 ps) and a longer decay component of 53 ± 3.6 ps (an average of four replicas). When monitored at 650 nm, assigned

Scheme 3. Proposed Double-Proton Transfer Model for DHNA in Cyclohexane

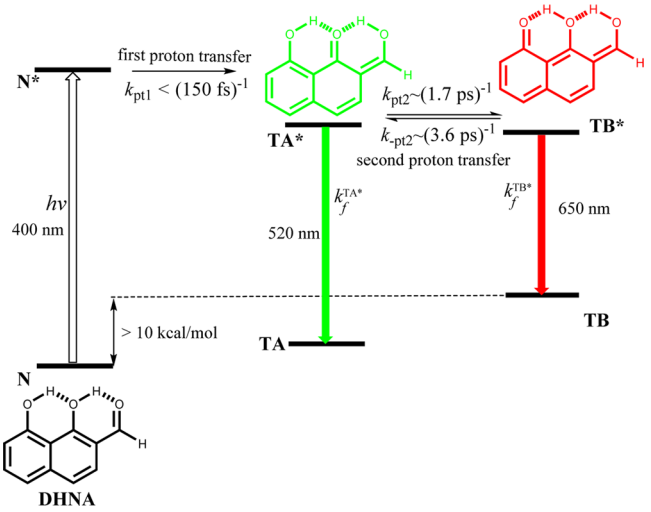

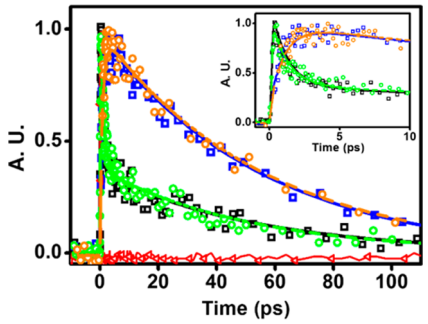

Figure 2. Time-resolved femtosecond fluorescence upconversion of **DHNA** in cyclohexane monitored at 520 nm (black open squares, □), 650 nm (blue open squares, □); deuterated **DHNA** in cyclohexane monitored at 520 nm (green open circles, ○) and 650 nm (orange open circles, ○). Solid (black and blue) and dashed lines (green and orange) depict the corresponding fitting curves; instrument response function is also shown (red). Inset: the depiction of relaxation dynamics within 10 ps.

to the TB* emission, the time trace apparently consists of a rise time of 1.1 ± 0.3 ps (a negative pre-exponential factor) and a decay component of 54 ± 3.2 ps (an average of four replicas). On the one hand, within experimental error, the shorter decay component of the TA* emission matches well to the rise component of the TB* emission. On the other hand, both TA* and TB* emissions show identical population decay times of ∼54 ps. The result clearly leads to the conclusions that TA* and TB* have a precursor−successor type of relationship and that these two species are in fast pre-equilibrium in the excited state. Because the rise component of TA* cannot be resolved, we conclude that the time scale of the first ESIPT from N* to TA* is beyond the instrument response function (IRF) of our current fluorescence upconversion setup (∼150 fs, monitored by Raman scattering signal at 428 nm (λ_{ex} = 400 nm) in cyclohexane). This viewpoint is also supported by monitoring the emission at close to 450 nm, which is supposed to be in the normal emission region and is obscure in the steady-state measurement; the upconverted signal is unresolvable from IRF (Figure S4).

The experimental results led us to conclude that a stepwise excited-state double-proton transfer reaction, consisting of an

DOI: 10.1021/jacs.5b08562
J. Am. Chem. Soc. 2015, 137, 14349−14357

ultrafast, system-unresolvable (<150 fs) ESIPT from N* to TA*, followed by a second forward-and-reverse proton transfer between TA* and TB*. As a result, the kinetic relationship among N*, TA*, and TB* can be described by the coupling reaction model depicted in Scheme 3. (See also Scheme S1.) Assuming that at $t \approx 0$ (<150 fs) that N* has been depopulated to ~0, under instant population of TA* and pseudoequilibrium between TA* and TB*, the time-resolved fluorescence intensity of TA* and TB*, denoted as $[TA^*]_f$ and $[TB^*]_f$, can be expressed by the following. (See eqs S1 for detailed derivation.)

$$[TA^*]_f = I_0 k_r^{TA^*}[TA^*]_{t=0} \left(\frac{k_{-pt2}}{k_{pt2} + k_{-pt2}} e^{-t/\tau_1} + \frac{k_{pt2}}{k_{pt2} + k_{-pt2}} e^{-t/\tau_2} \right)$$

$$[TB^*]_f = \frac{I_0 k_r^{TB^*} k_{pt2}[TA^*]_{t=0}}{(\tau_2)^{-1} - (\tau_1)^{-1}} (e^{-t/\tau_1} - e^{-t/\tau_2})$$

$$(\tau_1)^{-1} = \frac{k_f^{TA^*} + k_f^{TB^*} K_{eq}}{1 + K_{eq}}, \quad (\tau_2)^{-1} = k_{pt2} + k_{-pt2} \qquad (I)$$

where I_0 is a proportional constant incorporating instrument factor, k_r^{TA}* and k_r^{TB}* are the fluorescence radiative decay rate constants of TA* and TB*, respectively, and k_f^{TA}* and k_f^{TB}* are the sums of non-ESIPT decay rate constants for TA* and TB*, respectively. k_{pt2} denotes the forward (TA* → TB*) proton-transfer rate constant, and k_{-pt2} represents the reverse (TB* → TA*) proton-transfer rate constant. τ_2 and τ_1 are the observed decay time constants of the fast and slow decay components, respectively. As a result, the equilibrium constant $K_{eq} = k_{pt2}/k_{-pt2}$ can be obtained by the ratio of the pre-exponential factor (at $t = 0$) in eq I, which is deduced to be 2.13 (Figure 2), corresponding to a ΔG of −0.45 kcal/mol from TA* to TB*. Because $1/\tau_2$ is equivalent to $k_{pt2} + k_{-pt2}$, the forward-and-backward proton-transfer rate constants can be further deduced to be $k_{pt2} = (1.7\ ps)^{-1}$ and $k_{-pt2} = (3.6\ ps)^{-1}$. In a steady state manner, the TA* versus TB* ratiometric emission was also studied as a function of temperature. Upon lowering of the temperature from 303 to 243 K in methylcyclohexane, the results clearly show that TA* 520 nm emission gradually decreases, accompanied by an increase in the TB* 650 nm emission, supporting idea that the TB* species is thermally more stable (Figure 3A).

We also replaced the two protons of **DHNA** with deuterium and then studied the deuterium isotope effect on ESDPT. The result shown in Figure 2 reveals negligible changes of the fast decay (rise) component (~1.2 ps) of TA* (TB*). The deuterium-isotope-independent kinetics may, on the one hand, indicate that ESDPT is not directly coupled with the O−H stretching but rather induced by the motion of the molecular framework, most likely the low-frequency bending motion associated with changes in the angle and distance of the H bond. On the other hand, it may imply that the energy barrier is rather low and that the entropic or the recrossing effects dominate.[42,43] According to our transition state theory (TST)[44] calculation (page S23 of the Supporting Information), if the excited-state proton transfer reaction was dominantly controlled by the energy barrier and without recrossing the transition state region, then the deuterium kinetic isotope effect (KIE) would have been as high as 3.02 for the TA* → TB* reaction and k_{pt2} would have been at least seven times higher at 303 K.

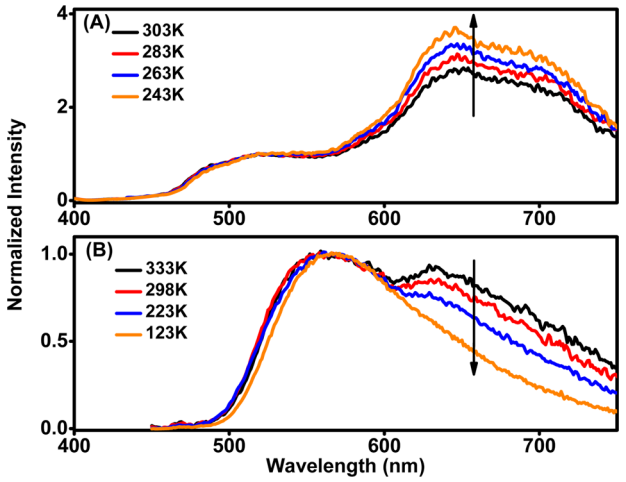

Figure 3. Temperature-dependent emission spectra of **DHNA** (A) in methylcyclohexane and (B) in a single crystal. Note that for comparison the emission is normalized at the maximum of the TA* emission.

ESDPT in Single Crystal. To make a direct correlation with the molecular structure, we also carried out spectroscopy and dynamics measurement in a single crystal. The emission of **DHNA** in a single crystal showed a similar double-proton transfer property, with the peak wavelengths located at 560 nm (TA*) and 650 nm (TB*), respectively (Figure 1). In the current stage, it is not feasible to apply fluorescence upconversion measurement for a single crystal of **DHNA** because we could not achieve the homogeneous excitation by the rotating sample cell to avoid thermal heating. Alternatively, the time-resolved studies were carried out using the time-correlated single-photon-counting (TCSPC) technique coupled with a femtosecond (~120 fs) laser pulse and a microchannel plate (MCP) detection system (Experimental Section). This combination allows a system response time of ~20 ps. The results shown in Figure S5 reveal that the TA* emission monitored at 520 nm consists of a fast relaxation decay (<system response time of 20 ps) and a longer decay component of 228 ± 20 ps. When monitored at 650 nm, assigned to the TB* emission, the time trace apparently consists of a system-unresolvable rise component (<20 ps) and a long decay component of 223 ± 22 ps. Within experimental errors, the population decay times of TA* and TB* are identical, supporting the fast equilibrium relationship concluded in solution. Interestingly, however, the thermodynamic relationship between TA* and TB* seems to be opposite to that observed in solution. Upon lowering of the temperature from 333 to 123 K in a single crystal, the results show that TA* 520 nm emission gradually increases, accompanied by the decrease of the TB* 650 nm emission (Figure 3B). The result leads to a more stable TA* species in the crystal, which is opposite to the more stable TB* species concluded in cyclohexane/methylcyclohexane. We thus believe that despite the establishment of equilibrium the relative thermodynamics are sensitive to environmental perturbation such as solvent polarity (in solution) or lattice (in crystal) stabilization.

Theoretical Investigation. We now present the computational approach in an aim to support the experimental observations. The calculated relative energies on the ground-

DOI: 10.1021/jacs.5b08562
J. Am. Chem. Soc. 2015, 137, 14349−14357

state (S_0) are listed in Table 1. The calculated molecular geometry and atom numbering are shown in Figure 4. The

Table 1. Calculated Ground-State (S_0) Energetics (kcal/mol) of DHNA System in Various Solvents

		cyclohexane	CH_2Cl_2	CH_3CN
B3LYP/6-31+G(d,p)	N[a]	0.00	0.00	0.00
	TS1	2.59	2.60	2.60
	TA	1.54	1.53	1.52
B3LYP/6-311+G(2df,2pd)//B3LYP/6-31+G(d,p)	N	0.00	0.00	0.00
	TS1	2.93	3.14	3.15
	TA	1.73	1.78	1.77
MP2/aug-cc-pVTZ//B3LYP/6-31+G(d,p)	N	0.00	0.00	0.00
	TS1	4.56	4.51	4.50
	TA	4.29	4.27	4.26
M06-2X/6-31+G(d,p)	N	0.00	0.00	0.00
	TS1	3.16	3.15	3.14
	TA	2.67	2.65	2.65

[a]N, TA, and TS1 represent the normal form, tautomer A, and transition state of N → TA, respectively.

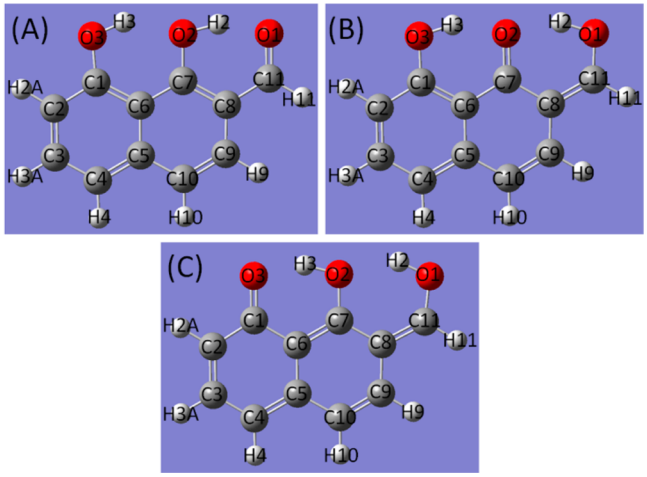

Figure 4. Calculated structures of (A) the normal form (N and N*), (B) tautomer A (TA and TA*), and (C) tautomer B (TB*) for the **DHNA** molecule.

calculated H-bond lengths of O(2)···H(3) and O(1)···H(2) of **DHNA** (Figure 4A) in cyclohexane are ∼0.12 Å shorter than those obtained by X-ray. Some of the calculated bond lengths are listed in Table S5. In the ground state (S_0), the normal form (N) is 1.5 kcal/mol lower in energy than tautomer A (TA), and the barrier of N → TA was 2.6 kcal/mol at the B3LYP[45]/6-31+G(d,p)[46] level in cyclohexane. The MP2[47] and M06-2X[48] calculations predicted only slightly higher barriers and energies of reactions. The calculated results in other solvents were very similar, as shown in Table 1.

Although it is true that TB can be drawn as a resonance Lewis structure of the normal form, the potential energy curve on S_0 along the TA → TB path (obtained from S_1), as shown in Figure S8, is monotonously uphill and does not form a localized potential energy well around TB. Thus, with the electron density distribution of S_0, the TB is a highly unstable structure. This has also been checked by MP2 calculation. However, on the first singlet excited-state (S_1) surface, the carbonyl group (C(7)═O(2)) of TA* becomes more electron-rich, which induces the second proton transfer and makes the TB structure a local energy minimum. It is not unusual that some of the proton-transfer tautomers exist only on the electronic excited state but not in the ground state if the normal form or other tautomers are much more stable in S_0.[49] The calculated relative energies of S_1 at the TD[50]-B3LYP/6-31+G(d,p) level in cyclohexane are shown in Table 2. In the first singlet excited-state (S_1), tautomer A (TA*) became the most stable isomer, and it was 2.4 and 1.8 kcal/mol lower in energy than the normal form (N*) and the tautomer B (TB*), respectively. The calculated barriers of N* → TA* and TA* → TB* were 0.3 and 2.1 kcal/mol, respectively.On the one hand, the results of the small energy difference (1.8 kcal/mol) between TA* and TB* support the existence of thermal equilibrium; on the other hand, the calculated TA* energy being lower than that of TB* is opposite to the experimental results. We attribute this discrepancy to the experimental and theoretical uncertainty, with the latter affected and limited by the theoretical level of the current computational approach. However, our EOM-CCSD[51] calculation suggests (Table 2) that TB* is 1.2 kcal/mol lower in energy than TA*, which is more consistent with the value deduced from the experiment. A similar discrepancy can be seen in the ground state. The tautomer TA is calculated

Table 2. Calculated First Excited State (S_1) Energetics (kcal/mol) of the DHNA System in Various Solvents

		cyclohexane	CH_2Cl_2	CH_3CN
TD-B3LYP/6-31+G(d,p)	N*[a]	0.00	0.00	0.00
	TS1*	0.27	0.30	0.31
	TA*	−2.38	−2.57	−2.61
	TS2*	−0.28	−0.84	−0.94
	TB*	−0.56	−1.76	−2.06
TD-B3LYP/6-311+G(2df,2pd)//TD-B3LYP/6-31+G(d,p)	N*	0.00	0.00	0.00
	TS1*	0.54	0.67	0.71
	TA*	−2.30	−2.20	−2.15
	TS2*	0.04	0.02	0.08
	TB*	−0.45	−1.03	−1.10
EOMCCSD/6-311+G(d,p)//TD-B3LYP/6-31+G(d,p)	N*	0.00	0.00	0.00
	TS1*	0.55	0.51	0.50
	TA*	−2.07	−2.11	−2.13
	TS2*	−1.01	−1.14	−1.23
	TB*	−3.26	−4.60	−4.96

[a]N*, TA*, TS1*, and TS2* represent the normal form*, tautomer A*, and transition states of N* → TA* and TA* → TB*, respectively.

DOI: 10.1021/jacs.5b08562
J. Am. Chem. Soc. 2015, 137, 14349−14357

to be only 1.5 kcal/mol higher in energy than that of the normal form (N), indicating the existence of trace TA under equilibrium. Experimentally, however, we could not resolve any corresponding TA spectrum. Nevertheless, even if it existed, because of the ultrafast N* → TA* ESIPT process, any direct excitation of trace TA should not affect the aforementioned double-proton transfer dynamics. In fact, the calculated energy of the transition state between N and TA is quite similar to that of TA (See Table 1). This suggests that with the inclusion of vibrational zero-point energy or at a higher-level calculation, N and TA might merge into a single potential energy well centered near N.

Despite the above discrepancies, the theoretical approach is consistent with the ultrafast first proton transfer and the slower second proton transfer indicated by experiment. The calculation using the larger basis set 6-311+G(2df,2dp) gave very similar results, though with slightly higher barriers. The TD-B3LYP/6-31+G(d,p) calculation predicted slightly lower barriers in dichloromethane and acetonitrile. A schematic plot showing the calculated relative energies on both S_0 and S_1 and the wavelengths of vertical excitation and emission in cyclohexane solvent at the B3LYP/6-31+G(d,p) and TD-B3LYP/6-31+G(d,p) levels are shown in Figure 5. It is noted

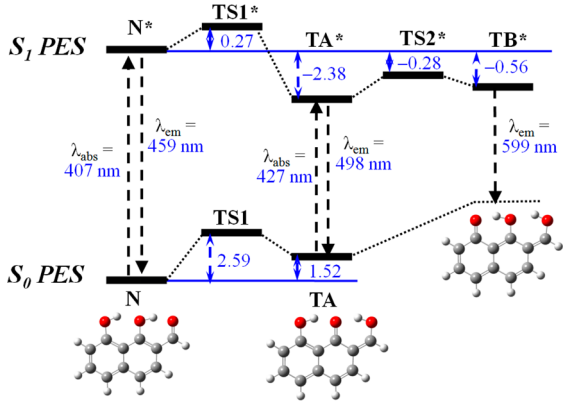

Figure 5. Calculated relative energies (kcal/mol) and wavelengths (nm) of vertical excitation and emission of the **DHNA** system in cyclohexane at the B3LYP/6-31+G(d,p) and TD-B3LYP/6-31+G(d,p) levels.

that the solvent effects need to be taken into account to find the TB* structure. In the gas-phase calculation, the TB* is not an energy minimum on the S_1 potential energy surface (PES). The calculated absorption wavelength (407 nm) of N was in good agreement with the experimental data. The calculated emission wavelengths from TA* and TB* were slightly shorter than the peak values of the experiments. It is, however, understandable because experimentally the emission corresponds to energy relaxation from the zero-point level of S_1 to various vibrational states on S_0, whereas the calculated values correspond to the differences in the underlying Born−Oppenheimer energies between S_1 and S_0 at the molecular geometries calculated on S_1. All the transitions between S_0 and S_1 were found to be of the HOMO → LUMO type. Similar schematic plots in dichloromethane and acetonitrile are included in the Supporting Information. Except for a 20 nm redshift in the emission of TB* from cyclohexane to acetonitrile, the calculated relative energies and the absorption/emission wavelengths were very similar in different solvents. Figure 6 shows a comprehensive 2D PES plot of both S_0 and S_1 in cyclohexane calculated at the

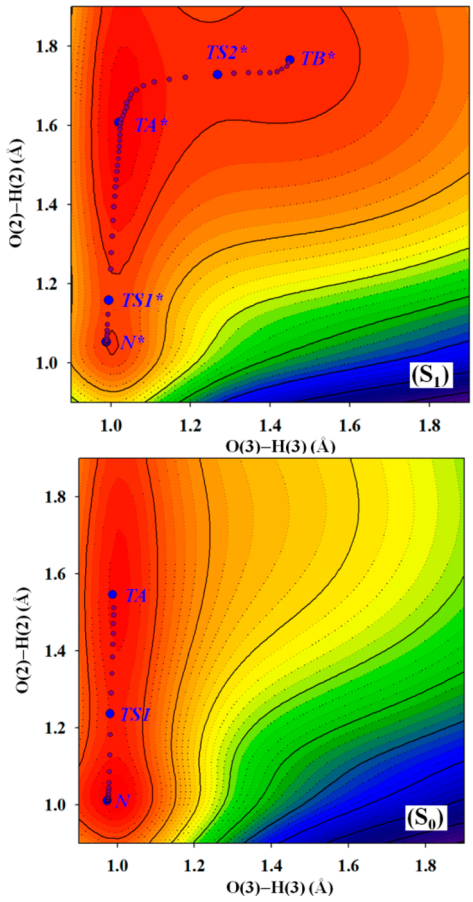

Figure 6. Calculated 2D potential energy maps of both the ground state (S_0) and the first excited state (S_1) for the proton-transfer reactions in the **DHNA** system in cyclohexane. The minimum energy path (solid purple circles) is also shown. The energy difference between neighboring dotted lines or color shades is 1 kcal/mol.

B3LYP/6-31+G(d,p) level. It clearly proves that in S_1 the sequential two-step proton motion is subject to the minimum energetic pathway consistent with the experimental results. It also showed that the region between the TA* and TB* was very smooth and low in energy on the S_1 surface. The calculated minimum energy path on S_1 indicated that the proton H(2) moves toward the O(1) in the first step which is followed by the transfer of H(3) to O(2). The electron density difference (EDD) maps between S_0 and S_1 as well as the HOMO and LUMO involved in the S_0−S_1 transitions for N and TA are plotted in Figure 7. As expected, the transitions are of the π−π^* type. The EDD maps in Figure 7 show that upon excitation from S_0 to S_1 there is a net electron density shift from the hydroxyl groups to the carbonyl oxygen (O(1) in N and O(2) in TA). This suggests that after the excitation a driving force was induced to facilitate the proton transfer reactions. This is consistent with the physical picture obtained from the HOMO−LUMO maps.

CONCLUSIONS

We have clearly shown that **DHNA**, containing dual intramolecular H bonds, undergoes a stepwise double-proton transfer. The first proton transfer (N* → TA*) is ultrafast, resulting in an O(2)-keto like tautomer emission maximized at 520 nm, whereas the second proton transfer (TA* → TB*) is fast but reversible, giving an O(3)-keto like tautomer form with

DOI: 10.1021/jacs.5b08562
J. Am. Chem. Soc. 2015, 137, 14349−14357

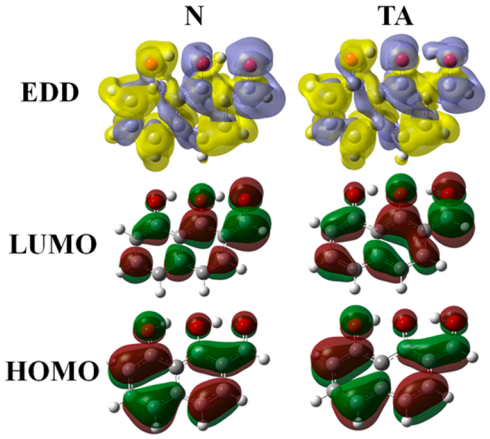

Figure 7. Calculated electron-density difference (EDD) maps between S_1 and S_0 and the HOMO (π)−LUMO (π^*) maps of the normal form (N) and tautomer A (TA) of the **DHNA** system in cyclohexane. In the EDD maps, the regions with increasing electron density from S_0 to S_1 are shown in violet, whereas the regions with decreasing density from S_0 to S_1 are shown in yellow.

emission at 650 nm. The experimental results are firmly supported by the theoretical calculation, which provides a comprehensive 2D PES plot associated with the double-proton transfer reaction, leading to the conclusion that the sequential two-step proton motion pathway is indeed along the minimum energy path.

During the past half century, excited-state intramolecular proton transfers have been the recognized models for finding fundamental regularities of the proton-transfer reactions that are basic to chemistry and biology. However, researchers have met with great difficulties in studying the case of multiple-proton transfers to mimic the biological proton-transfer system involving proton relay through hydrogen bonds. In this regard, the targeted synthesis of new doubly-hydrogen-bonded **DHNA** renders the paradigm to demonstrate unequivocally a stepwise, proton relay type of excited-state intramolecular double-proton transfer reaction.

EXPERIMENTAL SECTION

Synthesis and Characterization. All solvents were distilled from appropriate drying agents prior to use. Commercially available reagents were used without further purification unless otherwise stated. All reactions were monitored by TLC. Column chromatography was carried out using silica gel from Merck (230−400 mesh). ^{1}H and ^{13}C NMR spectra were recorded on a Varian Unity 400 spectrometer at 400 and 100 MHz, respectively. Chemical shifts (δ) are recorded in parts per million (ppm) and coupling constants (J) are reported in Hertz (Hz). Mass spectra were obtained using a gas chromatograph−mass spectrometer (Finnigan MAT TSQ-46C GC/MS/MS/DS).

Synthesis of 1,8-Bis(methylmethoxy)naphthalene (2). To a solution of naphthalene-1,8-diol (**1**) (1.60 g, 10 mmol) in DMF (12 mL) at 0 °C was added NaH (30 mmol), and the mixture was stirred for 1h. A solution of chloromethyl methyl ether (2.0 mL, 25 mmol) in Et_2O (10 mL) was added to the mixture. After stirring overnight, the reaction mixture was added to water and extracted with Et_2O (20 mL × 3). The organic extracts were combined, dried over anhydrous $MgSO_4$, filtered, and concentrated. The residue was purified using column chromatography on silica gel (DCM/hexanes) to yield **2** (2.11 g, 85%) as a white solid. ^{1}H NMR (400 MHz, $CDCl_3$, δ) 7.48 (dd, J = 8.0, 1.2 Hz, 2 H), 7.33 (t, J = 8.0 Hz, 2 H), 7.07 (dd, J = 8.0, 1.2 Hz, 2 H), 5.27 (s, 4 H), 3.57 (s, 6 H). ^{13}C NMR (100 MHz, $CDCl_3$, δ) 153.5, 137.7, 126.1, 122.7, 119.1, 112.7, 96.4, 56.3. ESI-MS m/z 248 (M^+).

Synthesis of 1,8-Bis(methoxymethoxy)-2-naphthaldehyde (3). A solution of compound **2** (1.36 g, 5.5 mmol) and Et_2O (10 mL) at 0 °C was added dropwise to a mixture of n-BuLi (2.5 M in hexane, 2.86 mL, 7.1 mmol) and TMEDA (1.06 mL, 7.1 mmol) in Et_2O (50 mL) and stirred for 6 h at this temperature. DMF (0.85 mL, 11 mmol) was added to the mixture for stirring overnight (0 °C to room temperature). Water was added to the mixture, and the pH was adjusted to 7 using 1.0 N HCl (aqueous). After extraction with Et_2O, the organic layer was dried over $MgSO_4$, filtered, and evaporated. The residue was purified using column chromatography on silica gel (DCM/hexanes/EA) to yield **3** (1.06 g, 70%) as an ochre solid. ^{1}H NMR (400 MHz, $CDCl_3$, δ) 10.57 (s, 1 H), 7.79 (d, J = 8.4 Hz, 1 H), 7.54 (d, J = 8.8 Hz, 1 H), 7.44−7.40 (m, 2H), 7.14 (m, 1H), 5.30 (s, 2 H), 5.18 (s, 2 H), 3.55 (s, 3 H), 3.52 (s, 3 H). ^{13}C NMR (100 MHz, $CDCl_3$, δ) 190.9, 159.1, 154.1, 140.2, 129.3, 127.0, 125.0, 122.5, 122.4, 119.4, 111.5, 101.9, 95.6, 57.9, 56.4. ESI-MS m/z 276 (M^+).

Synthesis of 1,8-Dihydroxy-2-naphthaldehyde (DHNA). A solution of compound **3** (0.28 g, 1.0 mmol) in CH_2Cl_2 (25 mL) at 0 °C was added dropwise to a mixture of isopropanol (6.4 mL) and HCl (4.8 mL). After stirring for 6 h, the solvent was removed under reduced pressure. The residue was purified using column chromatography on silica gel (DCM/hexanes) to yield **DHNA** (0.14 g, 75%) as a brownish-yellow solid. Mp = 138−139 °C (lit.[39] 139−140 °C). ^{1}H NMR (400 MHz, $CDCl_3$, δ) 14.29 (s, 1 H), 9.85 (s, 1 H), 9.40 (s, 1 H), 7.53 (t, J = 8.0 Hz, 1 H), 7.38 (d, J = 8.4 Hz, 1 H), 7.31 (d, J = 8.8 Hz, 1 H), 7.25 (d, J = 8.0 Hz, 1 H), 6.93 (d, J = 7.6 Hz, 1 H). ^{13}C NMR (100 MHz, $CDCl_3$) δ 195.9, 163.7, 157.7, 139.3, 132.7, 125.8, 120.5, 118.9, 113.2, 111.9. ESI-MS m/z 189 ($[M + H]^+$).

Spectroscopic Measurements. Steady-state absorption spectra were recorded using a Hitachi U-3310 Spectrophotometer, and emission spectra were obtained using an Edinburgh FS920 Fluorimeter. Detailed time-resolved spectroscopic measurements have been reported previously.[52] In brief, nanosecond time-resolved experiments were carried out by using an Edinburgh FLS920 time-correlated single-photon-counting (TCSPC) system with a pulsed hydrogen-filled lamp as the excitation source. Data were fitted with the sum of exponential functions using a nonlinear least-squares procedure in combination with a convolution method.

Subnanosecond to nanosecond time-resolved studies were carried out using another TCSPC system (OB-900 L lifetime spectrometer, Edinburgh) with an excitation light source from the second harmonic generation (SHG, 400 nm) of pulse-selected femtosecond laser pulses at 800 nm (Tsunami, Spectra-Physics) and a microchannel plate (MCP) detector. The fluorescence was collected at a right angle with respect to the pump beam path and passed through a polarizer, which was located in front of the detector. The polarization was set at a magic angle (54.7°) with respect to the pump polarization direction to eliminate anisotropy. Similar data analysis and fitting procedures were applied. The temporal resolution, after partial removal of the instrumental time broadening, was ∼20 ps.

Ultrafast spectroscopic study of the titled compounds was carried out by a femtosecond photoluminescence upconversion (uPL) system pumped at 400 nm. In this measurement, fluorescence from a rotating sample cell was focused in a BBO crystal, and its frequency was summed along with an interrogation gate pulse at a designated delay time with respect to the pump pulse. A half-wave plate was used to set the pump polarization at a magic angle (54.7°) with respect to the gate pulse to prevent the fluorescence anisotropy contributed by solute reorientation. Fluorescence upconversion data were fitted to the sum of exponential functions convoluted with the IRF. The IRF was determined from the Raman scattering signal, and its profile was fitted to a Gaussian function with a full width at half-maximum of ∼220 fs.

Computational Methodology. The structures and energies of 1,8-dihydroxy-2-naphthaldehyde (**DHNA**) and its tautomers in solvents were calculated by the hybrid density functionals B3LYP with the 6-31+G(d,p) basis set for the ground-state (S_0) potential energy surface (PES) and by the time-dependent (TD) B3LYP with the 6-31+G(d,p) basis set for the first singlet excited-state (S_1) PES

DOI: 10.1021/jacs.5b08562
J. Am. Chem. Soc. 2015, 137, 14349−14357

and the vertical $S_0 \rightarrow S_1$ excitation and the $S_1 \rightarrow S_0$ emissions. The above B3LYP/6-31+G(d,p) calculation on S_0 were checked by the single-point calculation at B3LYP/6-311+G(2df,2pd) and MP2/aug-cc-pVTZ level on the B3LYP/6-31+G(d,p) geometries and by the full calculation using the M06-2X functional with 6-31+G(d,p) basis set. The solvation effects in the solvent of cyclohexane, dichloromethane, and acetonitrile were considered by using the polarizable continuum model (PCM).[53] EOM-CCSD/6-311+G(d,p) calculation was also carried out to calculate the relative energies on the S_1 PES using the TD-B3LYP/6-31+G(d,p) geometries.

The transition state (TS) search was started from an educated guess on the TS structure by placing the hydrogen atom being transferred between the hydrogen donor and acceptor and by adjusting the bond lengths that are affected by the hydrogen transfer. Then, a Hessian calculation (second derivatives of energies with respect to the spatial coordinates) was carried out at the guessed TS structure to obtain the force constants. On the basis of the force constants, the TS search was carried out by the Berny optimization method.[54] The obtained TS was confirmed by carrying out a frequency calculation to see if only one imaginary frequency was obtained and that its vibrational eigenvector points to the correct direction. The rate constants and KIEs were obtained using the TST with the calculated geometries, vibrational frequencies, and barrier heights at the B3LYP/6-31+G(d,p) level. The 2D potential energy map (Figure 6) was calculated by setting the bond distances of O(2)−H(2) and O(3)−H(3) to various values that span the entire double-proton transfer processes. The other geometric degrees of freedom were optimized to achieve lowest possible energies (partial optimization). The energies thus-obtained were used to construct the map in Figure 6. The justification of this approach is that the two bond lengths are the most interesting and relevant coordinates in the proton transfer processes, and plotting the PES this way gave a clearer picture of the stepwise nature of the reactions. The other coordinates were allowed to relax during the calculation to obtain more reliable 2D PES. The full minimum-energy paths (the IRC calculation) of the N → TA, N* → TA*, and TA* → TB* reactions also have been calculated, and the correctness of the calculated TS were thus confirmed. The geometry on the paths was mapped to the 2D PES (Figure 6) and marked as solid purple circles. All the calculations were carried out using the Gaussian 09 program[55] except that the EOM-CCSD calculation was carried out using the MOLPRO program.[56]

■ ASSOCIATED CONTENT

Supporting Information

The Supporting Information is available free of charge on the ACS Publications website at DOI: 10.1021/jacs.5b08562.

Additional crystallographic and spectroscopic data. (PDF)

Crystallographic information file for **DHNA**. (CIF)

■ AUTHOR INFORMATION

Corresponding Authors

*Email: chewph@ccu.edu.tw (W.-P.H.).
*E-mail:chop@ntu.edu.tw (P.-T.C.).

Author Contributions

C.-Y.P. and J.-Y.S. contributed equally to this work.

Notes

The authors declare no competing financial interest.

■ ACKNOWLEDGMENTS

P.-T.C. and W.-P.H. thank the Ministry of Science and Technology, Taiwan, for financial support.

■ REFERENCES

(1) For the exceptional case, see Parada, G. A.; Markle, T. F.; Glover, S. D.; Hammarstrom, L.; Ott, S.; Zietz, B. *Chem. - Eur. J.* **2015**, *21*, 6362.
(2) Waluk, J. *Acc. Chem. Res.* **2003**, *36*, 832.
(3) Hsieh, C.-C.; Jiang, C.-M.; Chou, P.-T. *Acc. Chem. Res.* **2010**, *43*, 1364.
(4) Demchenko, A. P.; Tang, K. C.; Chou, P. T. *Chem. Soc. Rev.* **2013**, *42*, 1379.
(5) Tomin, V. I.; Demchenko, A. P.; Chou, P.-T. *J. Photochem. Photobiol., C* **2015**, *22*, 1.
(6) Chou, P.-T. *J. Chin. Chem. Soc.* **2001**, *48*, 651.
(7) Tolbert, L. M.; Solntsev, K. M. *Acc. Chem. Res.* **2002**, *35*, 19.
(8) Kwon, O. H.; Jang, D. J. *J. Phys. Chem. B* **2005**, *109*, 20479.
(9) Gelabert, R.; Moreno, M.; Lluch, J. M. *J. Phys. Chem. A* **2006**, *110*, 1145.
(10) Zhao, J.; Ji, S.; Chen, Y.; Guo, H.; Yang, P. *Phys. Chem. Chem. Phys.* **2012**, *14*, 8803.
(11) Chou, H. C.; Hsu, C. H.; Cheng, Y. M.; Cheng, C. C.; Liu, H. W.; Pu, S. C.; Chou, P. T. *J. Am. Chem. Soc.* **2004**, *126*, 1650.
(12) Gao, M.; Hu, Q.; Feng, G.; Tang, B. Z.; Liu, B. *J. Mater. Chem. B* **2014**, *2*, 3438.
(13) Tang, K.-C.; Chang, M.-J.; Lin, T.-Y.; Pan, H.-A.; Fang, T.-C.; Chen, K.-Y.; Hung, W.-Y.; Hsu, Y.-H.; Chou, P.-T. *J. Am. Chem. Soc.* **2011**, *133*, 17738.
(14) Kwon, J. E.; Park, S. Y. *Adv. Mater.* **2011**, *23*, 3615.
(15) Demchenko, A. P. *FEBS Lett.* **2006**, *580*, 2951.
(16) Rodriguez-Rodriguez, C.; Sanchez de Groot, N.; Rimola, A.; Alvarez-Larena, A.; Lloveras, V.; Vidal-Gancedo, J.; Ventura, S.; Vendrell, J.; Sodupe, M.; Gonzalez-Duarte, P. *J. Am. Chem. Soc.* **2009**, *131*, 1436.
(17) Wierzchowski, J. *Nucleosides, Nucleotides Nucleic Acids* **2014**, *33*, 626.
(18) Lee, M. H.; Kim, J. S.; Sessler, J. L. *Chem. Soc. Rev.* **2015**, *44*, 4185.
(19) Agmon, N. *Chem. Phys. Lett.* **1995**, *244*, 456.
(20) Taylor, C. A.; El-Bayoumi, M. A.; Kasha, M. *Proc. Natl. Acad. Sci. U. S. A.* **1969**, *63*, 253.
(21) Mente, S.; Maroncelli, M. *J. Phys. Chem. A* **1998**, *102*, 3860.
(22) Chou, P. T.; Yu, W. S.; Wei, C. Y.; Cheng, Y. M.; Yang, C. Y. *J. Am. Chem. Soc.* **2001**, *123*, 3599.
(23) Gai, F.; Rich, R. L.; Petrich, J. W. *J. Am. Chem. Soc.* **1994**, *116*, 735.
(24) Negrerie, M.; Gai, F.; Bellefeuille, S. M.; Petrich, J. W. *J. Phys. Chem.* **1991**, *95*, 8663.
(25) Chou, P. T.; Martinez, M. L.; Cooper, W. C.; Collins, S. T.; McMorrow, D. P.; Kasha, M. *J. Phys. Chem.* **1992**, *96*, 5203.
(26) Chen, Y.; Rich, R. L.; Gai, F.; Petrich, J. W. *J. Phys. Chem.* **1993**, *97*, 1770.
(27) Smirnov, A. V.; English, D. S.; Rich, R. L.; Lane, J.; Teyton, L.; Schwabacher, A. W.; Luo, S.; Thornburg, R. W.; Petrich, J. W. *J. Phys. Chem. B* **1997**, *101*, 2758.
(28) Wu, Y. S.; Huang, H. C.; Shen, J. Y.; Tseng, H. W.; Ho, J. W.; Chen, Y. H.; Chou, P. T. *J. Phys. Chem. B* **2015**, *119*, 2302.
(29) Takeuchi, S.; Tahara, T. *Proc. Natl. Acad. Sci. U. S. A.* **2007**, *104*, 5285.
(30) Kwon, O. H.; Zewail, A. H. *Proc. Natl. Acad. Sci. U. S. A.* **2007**, *104*, 8703.
(31) Catalan, J. *Proc. Natl. Acad. Sci. U. S. A.* **2008**, *105*, E78. (Author reply, E79)
(32) Kwon, O.-H.; Zewail, A. H. *Proc. Natl. Acad. Sci. U. S. A.* **2008**, *105*, E79.
(33) Bulska, H. *Chem. Phys. Lett.* **1983**, *98*, 398.
(34) Zhang, H.; van der Meulen, P.; Glasbeek, M. *Chem. Phys. Lett.* **1996**, *253*, 97.
(35) Toele, P.; Zhang, H.; Glasbeek, M. *J. Phys. Chem. A* **2002**, *106*, 3651.
(36) Plasser, F.; Barbatti, M.; Aquino, A. J. A.; Lischka, H. *J. Phys. Chem. A* **2009**, *113*, 8490.

DOI: 10.1021/jacs.5b08562
J. Am. Chem. Soc. 2015, 137, 14349−14357

(37) Tang, K.-C.; Chen, C.-L.; Chuang, H.-H.; Chen, J.-L.; Chen, Y.-J.; Lin, Y.-C.; Shen, J.-Y.; Hu, W.-P.; Chou, P.-T. *J. Phys. Chem. Lett.* **2011**, *2*, 3063.
(38) Glaser, T.; Liratzis, I.; Frohlich, R. *J. Chem. Soc., Dalton Trans.* **2005**, 2892.
(39) Guo, Z.-Q.; Chen, W.-Q.; Duan, X.-M. *Org. Lett.* **2010**, *12*, 2202.
(40) Tobita, S.; Yamamoto, M.; Kurahayashi, N.; Tsukagoshi, R.; Nakamura, Y.; Shizuka, H. *J. Phys. Chem. A* **1998**, *102*, 5206.
(41) Singh, R. B.; Mahanta, S.; Kar, S.; Guchhait, N. *Chem. Phys.* **2007**, *331*, 373.
(42) O'Leary, D. J.; Hickstein, D. D.; Hansen, B. K. V.; Hansen, P. E. *J. Org. Chem.* **2010**, *75*, 1331.
(43) Hu, W.-P.; Truhlar, D. G. *J. Am. Chem. Soc.* **1995**, *117*, 10726.
(44) Truhlar, D. G.; Garrett, B. C. *Acc. Chem. Res.* **1980**, *13*, 440.
(45) Becke, A. D. *J. Chem. Phys.* **1993**, *98*, 5648.
(46) Frisch, M. J.; Pople, J. A.; Binkley, J. S. *J. Chem. Phys.* **1984**, *80*, 3265.
(47) Møller, C.; Plesset, M. S. *Phys. Rev.* **1934**, *46*, 618.
(48) Zhao, Y.; Truhlar, D. G. *Theor. Chem. Acc.* **2008**, *120*, 215.
(49) Hu, W.-P.; Chen, J.-L.; Hsieh, C.-C.; Chou, P.-T. *Chem. Phys. Lett.* **2010**, *485*, 226.
(50) Scalmani, G.; Frisch, M. J.; Mennucci, B.; Tomasi, J.; Cammi, R.; Barone, V. *J. Chem. Phys.* **2006**, *124*, 094107.
(51) Kállay, M.; Gauss, J. *J. Chem. Phys.* **2004**, *121*, 9257.
(52) Chou, P. T.; Pu, S. C.; Cheng, Y. M.; Yu, W. S.; Yu, Y. C.; Hung, F. T.; Hu, W. P. *J. Phys. Chem. A* **2005**, *109*, 3777.
(53) Tomasi, J.; Mennucci, B.; Cammi, R. *Chem. Rev.* **2005**, *105*, 2999.
(54) Schlegel, H. B. *J. Comput. Chem.* **1982**, *3*, 214.
(55) Frisch, M. J.; Trucks, G. W.; Schlegel, H. B.; Scuseria, G. E.; Robb, M. A.; Cheeseman, J. R.; Scalmani, G.; Barone, V.; Mennucci, B.; Petersson, G. A.; Nakatsuji, H.; Caricato, M.; Li, X.; Hratchian, H. P.; Izmaylov, A. F.; Bloino, J.; Zheng, G.; Sonnenberg, J. L.; Hada, M.; Ehara, M.; Toyota, K.; Fukuda, R.; Hasegawa, J.; Ishida, M.; Nakajima, T.; Honda, Y.; Kitao, O.; Nakai, H.; Vreven, T.; Montgomery, J. A., Jr.; Peralta, J. E.; Ogliaro, F.; Bearpark, M.; Heyd, J. J.; Brothers, E.; Kudin, K. N.; Staroverov, V. N.; Kobayashi, R.; Normand, J.; Raghavachari, K.; Rendell, A.; Burant, J. C.; Iyengar, S. S.; Tomasi, J.; Cossi, M.; Rega, N.; Millam, J. M.; Klene, M.; Knox, J. E.; Cross, J. B.; Bakken, V.; Adamo, C.; Jaramillo, J.; Gomperts, R.; Stratmann, R. E.; Yazyev, O.; Austin, A. J.; Cammi, R.; Pomelli, C.; Ochterski, J. W.; Martin, R. L.; Morokuma, K.; Zakrzewski, V. G.; Voth, G. A.; Salvador, P.; Dannenberg, J. J.; Dapprich, S.; Daniels, A. D.; Farkas, O.; Foresman, J. B.; Ortiz, J. V.; Cioslowski, J.; Fox, D. J. *Gaussian 09*, revision D. 01; Gaussian, Inc.: Wallingford, CT, 2009.
(56) Werner, H.; Knowles, P.; Knizia, G.; Manby, F.; Schütz, M.; Celani, P.; Korona, T.; Lindh, R.; Mitrushenkov, A.; Rauhut, G. *MOLPRO*; University College Cardiff Consultants, Ltd.: Wales, U.K., 2012.

DOI: 10.1021/jacs.5b08562
J. Am. Chem. Soc. 2015, 137, 14349−14357